J. Mech. Phys. Solids 173 (2023) 105223

Contents lists available at ScienceDirect

Journal of the Mechanics and Physics of Solids

journal homepage: www.elsevier.com/locate/jmps

Why does an elastomer layer confined between two rigid blocks grow numerous cavities?

Sida Hao [a], Zhigang Suo [b], Rui Huang [a,*]

[a] Department of Aerospace Engineering and Engineering Mechanics, University of Texas, Austin, TX 78712, United States
[b] John A. Paulson School of Engineering and Applied Sciences, Harvard University, MA 02138, United States

ARTICLE INFO

Keywords:
Cavitation
Fracture
Elastomer

ABSTRACT

For a thin layer of elastomer sandwiched between two rigid blocks, when the blocks are pulled, numerous cavities grow in the elastomer like cracks. Why does the elastomer grow numerous small cracks instead of a single large crack? Here we answer this question by analyzing an idealized model, in which the elastomer is an incompressible neoHookean material and contains a penny-shaped crack. To simulate one representative crack among many, the model is axisymmetric with zero radial displacement at the edge. When the rigid blocks are pulled by a pair of forces, a hydrostatic tension develops in the elastomer. At a critical hydrostatic tension, a small crack deforms substantially, as predicted by an elastic instability, resulting in an unbounded energy release rate. Consequently, the small crack initiates its growth, regardless of the toughness of the elastomer. As the crack grows, the energy release rate decreases, so that the crack arrests. Meanwhile, the rigid blocks constrain deformation of the elastomer far away from the crack, where hydrostatic tension remains high, allowing other cracks to grow. For an elastomer of thickness H, shear modulus μ, and toughness G_c, the crack radius and spacing decrease as the normalized toughness $G_c/(\mu H)$ increases. Therefore, a tough elastomer of small modulus and thickness will grow numerous small cracks when confined by two rigid blocks and pulled beyond a critical force.

1. Introduction

Consider a layer of elastomer bonded between two blocks of metal, with the thickness of the elastomer being much smaller than its diameter, $H << D$ (Fig. 1a). When the two metal blocks are pulled by a pair of sufficiently large forces, F, the elastomer forms numerous cavities (Fig. 1b) (Gent and Lindley, 1959). The metal is much stiffer than the elastomer, and is regarded as a rigid material. The metal blocks adhere well to the elastomer, and constrain deformation of the elastomer in transverse directions. Consequently, the longitudinal force F induces a field of triaxial stress in the elastomer. Gent and Lindley (1959) modeled the elastomer as an incompressible neoHookean material of shear modulus μ, subject to a hydrostatic tensile stress σ. They identified an elastic instability: a pre-existing defect in the elastomer deforms into a cavity of arbitrarily large radius at a critical hydrostatic stress, $\sigma_c = 2.5\mu$. They used this elastic instability to interpret the onset of cavitation in their experiments. Postmortem examination showed no visible damage in the elastomer below a critical force, but numerous cracks above. In experiments using a transparent elastomer, they observed that the elastomer formed many small spherical cavities. Upon unloading, the cavities became crack-like. In their thinnest specimen ($D/H \sim 35$),

* Corresponding author.
E-mail address: ruihuang@mail.utexas.edu (R. Huang).

https://doi.org/10.1016/j.jmps.2023.105223
Received 12 October 2022; Received in revised form 13 January 2023; Accepted 21 January 2023
Available online 23 January 2023

many small cracks distributed throughout the mid-plane of the specimen, with the crack size and spacing comparable to the elastomer thickness.

Why does the elastomer grow numerous small cracks instead of a single large crack? Here we seek to answer this question using an idealized model (Fig. 2). We represent the elastomer as an incompressible neoHookean material, containing pre-existing penny-shaped cracks much smaller than the thickness of the elastomer. Picture that the cracks form a hexagonal array, so that the deformation of the elastomer can be analyzed by a hexagonal unit cell with periodic boundary conditions. To further idealize the model, we approximate the hexagonal unit cell by a circular cell of radius B in an axisymmetric model with a single crack of radius C, in an elastomer disk of thickness H, bonded between two rigid blocks. Both radii, C and B, are measured in the undeformed state. The diameter of the cell, $2B$, approximately represents the spacing between adjacent cracks. The radial displacement at the edge of the elastomer disk ($R = B$) is set to zero, mimicking a symmetry boundary condition between adjacent cracks, so that the axisymmetric model approximately accounts for the interactions between the neighboring cracks. The rigid blocks are pulled by prescribing a displacement Δ, and we calculate the applied force F, the energy release rate G of the crack, and the hydrostatic stress σ_{edge} at the edge of the elastomer disk. We find that G becomes unbounded at a critical force, so that the crack grows, regardless of the toughness of the elastomer. As the crack radius increases, G decreases, so that the crack arrests. Because the rigid blocks constrain the deformation of the elastomer far away from the crack, σ_{edge} can be large enough for other cracks to grow. For an elastomer of thickness H, shear modulus μ, and toughness G_c, a dimensionless group, $G_c/(\mu H)$, is identified. A specimen with a large value of $G_c/(\mu H)$ ruptures by forming numerous small cracks. In contrast, a specimen with a small value of $G_c/(\mu H)$ ruptures by forming a single large crack.

Previous studies on cavitation in elastomers have been reviewed in several recent papers (Lefevre et al., 2015; Raayai-Ardakani et al., 2019a, 2019b; Barney et al., 2020; Kim et al., 2020; Morelle et al., 2021; Kumar and Lopez-Pamies, 2021). The classical cavitation theory based on elastic instability predicts that a spherical cavity in an elastomer expands unstably at a critical hydrostatic stress proportional to the shear modulus of the elastomer (Gent and Lindley, 1959). This prediction neglects the nucleation stage of cavitation and assumes pre-existing defects in the elastomer. In a later paper, Gent (1990) offered a cautionary tale about interpreting the observed cavitation purely on the basis of the elastic instability. Because the observed cavities are large compared to typical initial defects, some polymer chains must be broken during cavitation. It has long been suggested that cavities grow like cracks in an elastomer (Gent, 1990; Kundu and Crosby, 2009; Lefevre et al., 2015; Poulain et al., 2017; Hutchens et al., 2016; Kang et al., 2017; Raayai-Ardakani et al., 2019b).

More recently, it has been suggested that a cavity grows in an elastomer by distributed scission of polymer chains (Kim et al., 2020; Morelle et al., 2021). Here we assume that a cavity grows like a penny-shaped crack, and study the consequence of this assumption. Several previous works considered a penny-shaped crack in an infinite body subject to hydrostatic tension (Williams and Schapery, 1965; Gent and Wang, 1991; Lin and Hui, 2004; Long and Hui, 2010). Because the radius of the crack is the only length in such a model, the energy release rate is linear in the radius. For an incompressible neoHookean material, this model predicts that the energy release rate of the crack becomes unbounded when the hydrostatic tension approaches a critical value, $\sigma_c = 2.5\mu$, which coincides with the critical stress for the elastic instability of a spherical cavity. Assuming a constant toughness for the elastomer, the model therefore predicts that a pre-existing defect of any size would grow unstably in an infinite body at the critical hydrostatic tension. However, experimental observations suggest that the crack growth is stabilized in a thin layer of elastomer constrained between two rigid blocks, provided that the ratio D/H is large (Fig. 1) (Gent and Lindley, 1959). The constraint by the two rigid blocks introduces another length scale, H, the thickness of the elastomer layer. As noted earlier, this constraint arrests the crack, but still permits high hydrostatic tension in the elastomer far away from the crack, causing numerous cracks to grow. Such stable growth of numerous cracks has been simulated by a phase field model (Kumar and Lopez-Pamies, 2021). Here we study the phenomenon using a nonlinear elastic fracture mechanics approach.

2. An axisymmetric crack model

Fig. 2 illustrates the axisymmetric model with a penny-shaped crack. The upper and lower surfaces of the elastomer are tied to the rigid blocks that are pulled away from each other, by prescribing a displacement Δ. The elastomer is modeled as an incompressible neoHookean material, and geometric nonlinearity is considered for large deformation. For each model with selected values of B/H and C/H, a quasi-static finite element analysis is performed using ABAQUS, and the energy release rate of the crack is calculated using the

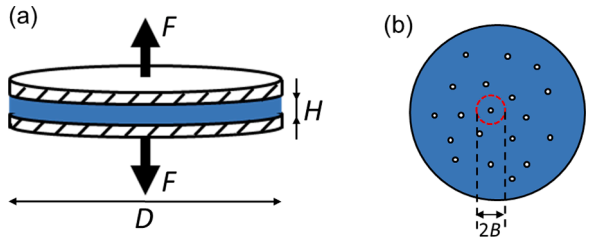

Fig. 1. (a) Schematics of an experiment, in which a layer of elastomer of thickness H and diameter D ($D >> H$) is sandwiched between two rigid blocks, pulled by a pair of forces F. (b) Numerous cavities grow like cracks in the elastomer. The spacing between adjacent cavities is approximately $2B$, and one of the cavities is circled as a representative cell for analysis.

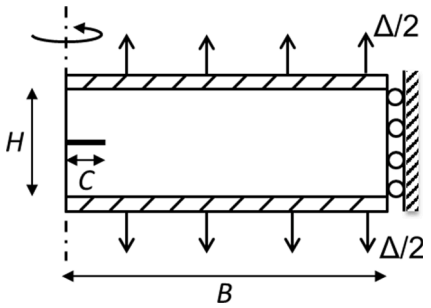

Fig. 2. Schematic of an axisymmetric model in the undeformed state, with a penny-shaped crack lying on the middle plane of a layer of elastomer sandwiched between two rigid blocks. The two rigid blocks are pulled to a separation displacement Δ. The radial displacement at the edge of the elastomer is set to zero, mimicking a symmetry boundary condition between adjacent cracks. In the finite element analysis, only the upper half of the elastomer layer is meshed, assuming symmetry for the lower half.

J-integral method. Axisymmetric second-order elements are used, with quarter-point singular elements at the crack front to mitigate the stress singularity. Once Δ/H, B/H, and C/H are specified, the finite element model calculates the normalized applied force $F/(\pi B^2\mu)$, the normalized energy release rate $G/(\mu H)$, and the normalized hydrostatic stress at the edge σ_{edge}/μ.

In experiments, even before cavitation, the elastomer deforms inhomogeneously due to the free edge ($R = D/2$) (Fig. 1). For a thin specimen ($H << D$) and an incompressible neoHookean material, the stress field is nearly uniform in the center region, with the magnitude of the hydrostatic stress being twice of the applied force divided by the area of the specimen (Gent and Lindley, 1959). Here, the idealized axisymmetric model simulates one representative cavity in the center region, far away from the free edge ($B << D$). Therefore, the normalized force in the axisymmetric model, $F/(\pi B^2\mu)$, is approximately twice of the normalized force applied to the specimen in corresponding experiments. Moveover, we have chosen to focus on the cases when many small cavities were observed in experiments, typically for thin specimens ($H << D$). In such specimens, the small cavities appeared to be penny-shaped cracks growing in the horizontal direction. More complicated crack growth may occur in relatively thick specimens, which cannot be treated in the present model.

3. Initiation of crack growth

We first study the initiation of crack growth from a pre-existing crack, which is taken to be small compared to the layer thickness, $C/H = 0.01$. For such a small crack, the normalized force-displacement curve is nearly a step function (Fig. 3). When the normalized force is below the critical value for elastic instability, $F/(\pi B^2\mu) < 2.5$, the deformation is small everywhere except for the neighborhood around the small crack, as shown by the inset at $F/(\pi B^2\mu) = 2$. Since the elastomer is modeled as an incompressible material, the normalized displacement Δ/H is nearly zero when $F/(\pi B^2\mu) < 2.5$. As $F/(\pi B^2\mu)$ approaches 2.5, the elastomer around the crack deforms substantially, as predicted by the elastic instability, so that the normalized displacement Δ/H increases rapidly at $F/(\pi B^2\mu) \approx 2.5$. As shown by the inset at $F/(\pi B^2\mu) = 2.5$, even with a small applied displacement, $\Delta/H \sim 0.004$, the initially small crack

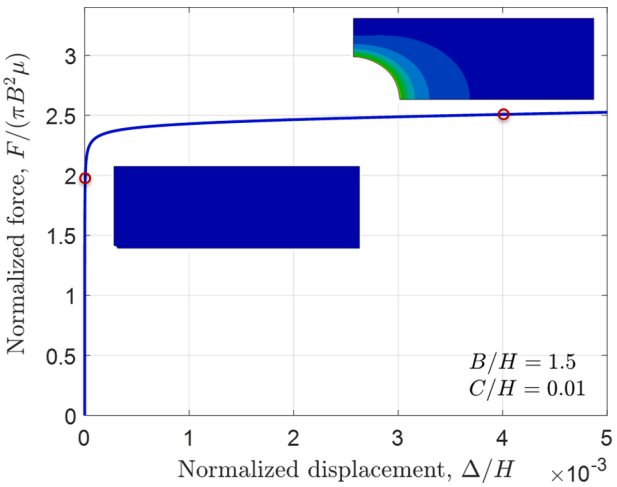

Fig. 3. Deformation of an elastomer layer containing a small crack ($C/H = 0.01$). The force-displacement curve is nearly a step function. The insets show two states of deformation with contours of displacement amplitude. At $F/(\pi B^2\mu) = 2$, the deformation around the crack is relatively small. At $F/(\pi B^2\mu) = 2.5$, the initially small crack deforms into a large cavity.

deforms into a large cavity. This large deformation involves no crack growth in the finite element calculation.

Corresponding to the elastic deformation in Fig. 3, the normalized energy release rate, $G/(\mu H)$, increases significantly with a small increase in the displacement Δ/H (Fig. 4a). We also plot $G/(\mu H)$ versus the normalized force, $F/(\pi B^2\mu)$ (Fig. 4b). The energy release rate remains small when $F/(\pi B^2\mu) < 2.5$, but increases dramatically at $F/(\pi B^2\mu) \to 2.5$. This result is similar to the energy release rate of a penny-shaped crack in an infinite elastomer subject to hydrostatic tension (Lin and Hui, 2004; Kang et al., 2017). As the normalized force exceeds 2.5, the finite element calculation is terminated due to numerical divergence, indicative of a singular, unbounded energy release rate. By the Griffith criterion for fracture, the crack grows when the energy release rate reaches the material toughness, $G = G_c$. So long as the pre-existing crack is small compared to the elastomer thickness, $C/H << 1$, the *G-F* relation is nearly a step function. Consequently, the small crack starts to grow when $F/(\pi B^2\mu) \approx 2.5$. This critical force is dictated by the elastic instability of a small defect, and is independent of the toughness G_c.

4. Crack arrest

We repeat the finite element calculations for several values of the normalized crack radius C/H, with a fixed value of $B/H = 1.5$. Again, for each C/H, we prescribe the normalized displacement Δ/H, and calculate the normalized force $F/(\pi B^2\mu)$, and the normalized energy release rate $G/(\mu H)$. We plot the results as normalized force-displacement curves (Fig. 5a). The solid curves are the force-displacement curves when the radius of the crack is fixed at various values. For a small crack, $C/H = 0.01$, the calculation diverges beyond a small displacement, and the force-displacement curve appears like a vertical line, which terminates approximately at the critical force of elastic instability, $F/(\pi B^2\mu) = 2.5$. For a larger crack, say $C/H = 0.1$, the force-displacement curve becomes smooth and readily continues beyond the critical force of elastic instability. For a given displacement, the larger the crack radius, the lower the force.

We next consider the growth of the crack. Assume that the crack grows when the energy release rate exceeds a constant value of toughness, $G \geq G_c$. For a prescribed B/H, we vary C/H and Δ/H to calculate the applied force and energy release rate as functions, $F(\Delta/H, C/H)$ and $G(\Delta/H, C/H)$. Given a toughness G_c, the critical condition for crack growth, $G(\Delta/H, C/H) = G_c$, gives the crack radius C/H as a function of Δ/H (Fig. 5b), and a dashed curve on the force-displacement plane (Fig. 5a). This dashed curve is the normalized force-displacement curve when the crack grows under the condition $G = G_c$. For a tough elastomer, $G_c/(\mu H) = 2$, as the displacement increases, initially the crack grows slightly and the force increases, and then the crack grows more significantly and the force decreases. For a brittle elastomer, $G_c/(\mu H) = 0.3$, as the displacement increases, the crack grows rapidly upon initiation, and the force decreases sharply. The two types of force-displacement curves roughly correspond to the behaviors of brittle and tough elastomers, such as the single-network and double/triple-network elastomers considered by Morelle et al. (2021).

Recall that the finite element method calculates the function $G(\Delta/H, C/H)$ using a model of fixed displacement and crack radius. This function is plotted as *G-C* curves on the plane of energy release rate and crack radius for several values of Δ/H (Fig. 6). Examine a *G-C* curve at a fixed displacement in the two limits of the crack radius. In one limit, $C \to 0$, as noted before, due to the elastic instability, any finite displacement leads to an unbounded energy release rate, $G \to \infty$. In the other limit, $C \to B$, the width of elastomer ligament ahead of the crack, $B - C$, is the only relevant length scale in the boundary value problem, so that the energy release rate is linear in $B - C$, and thus $G \to 0$. At a fixed displacement, the *G-C* curve is a monotonically decreasing curve between the two limits. For a small displacement, $\Delta/H = 0.001$, the *G-C* curve is nearly L-shaped: The energy release rate approaches infinity as $C/H \to 0$, and drops sharply to almost zero as C/H increases. For a larger displacement, the *G-C* curve decreases more gently.

At a fixed displacement, the monotonically decreasing *G-C* curve ensures the arrest of the crack. For a given toughness, which is

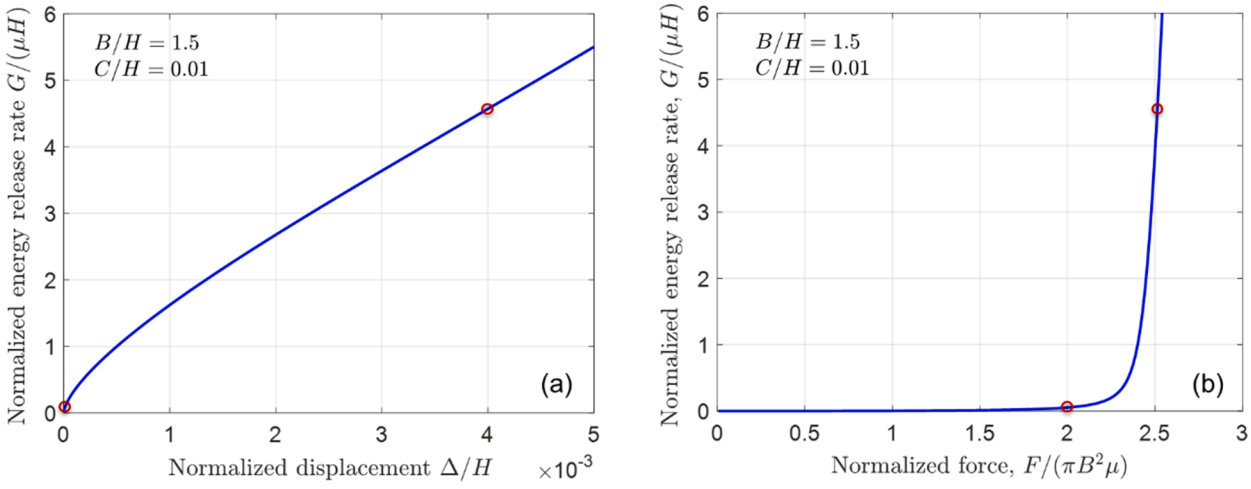

Fig. 4. Energy release rate of a small crack ($C/H = 0.01$) in an elastomer layer. (a) The normalized energy release rate increases with the applied displacement. (b) The energy release rate is nearly a step function of the applied force, and becomes unbounded at $F/(\pi B^2\mu) \approx 2.5$.

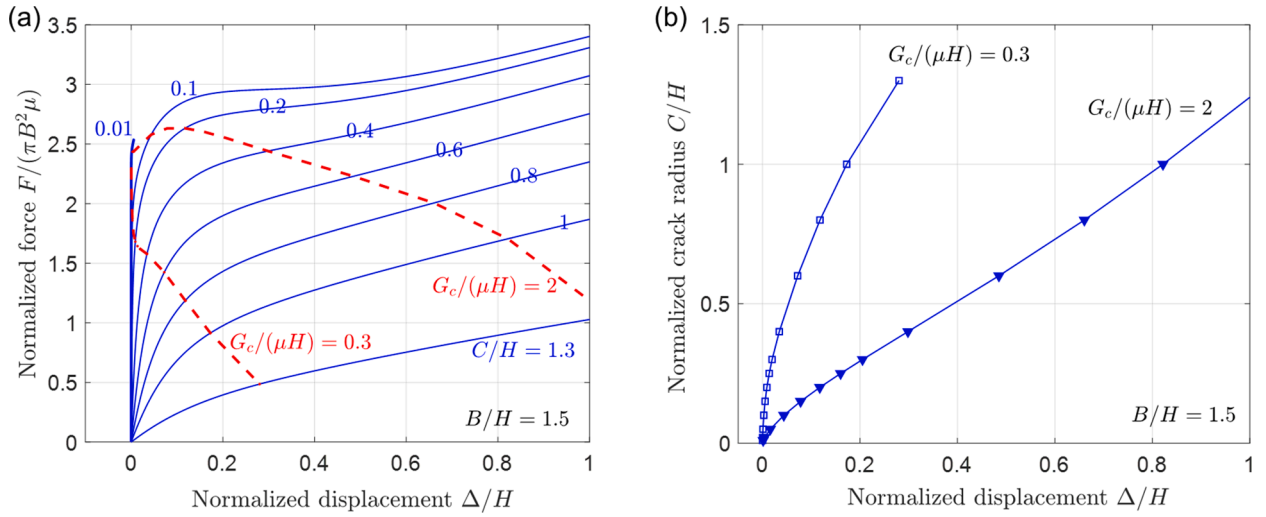

Fig. 5. (a) Normalized force-displacement curves. Each solid curve is a force-displacement curve for a crack of a fixed radius. Each dashed curve is a force-displacement curve as the crack grows under the condition $G = G_c$. (b) Normalized radius of an arrested crack for two different values of toughness.

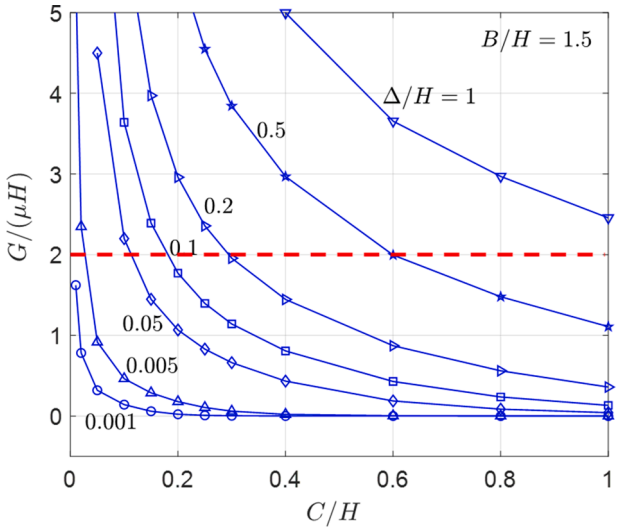

Fig. 6. Normalized *G-C* curves. For a fixed displacement, the energy release rate decreases monotonically as the crack radius increases. The horizontal dashed line represents a constant toughness. At a given displacement, each *G-C* curve intersects with the horizontal dashed line at one point, which gives the radius of an arrested crack.

marked as a horizontal dashed line in Fig. 6, the critical condition of crack growth, $G = G_c$, is met at the intersections between the horizontal line and the *G-C* curves. Each intersection gives the radius C/H of an arrested crack at a fixed displacement Δ/H. The crack cannot grow any further because the energy release rate would drop below G_c unless Δ/H increases. The radius of the arrested crack increases with Δ/H (Fig. 5b).

The deformation of the elastomer depends on the radius of the crack and applied displacement (Fig. 7). Snapshots of the deformed elastomer are presented at four crack radii and two energy release rates. Marked in each snapshot is the corresponding applied displacement. We interpret each column as the snapshots of a crack growing in an elastomer of a constant toughness G_c. At a small applied displacement, the crack is small, $C/H \to 0$, and the elastomer is mostly undeformed, except for the highly localized deformation around the crack. As the applied displacement increases, the crack grows, and the entire elastomer deforms substantially. As $C \to B$, the ligament ahead of the crack is highly stretched. Because the computational model is axisymmetric, the ligament ahead of the crack is stretched into a thin sheet, where the radial stress is nearly zero due to the traction-free crack face. The deformation of the ligament is constrained in the circumferential direction, and stretched in the vertical direction. That is, the thin sheet is stretched under a plane strain condition, similar to that in a pure shear test.

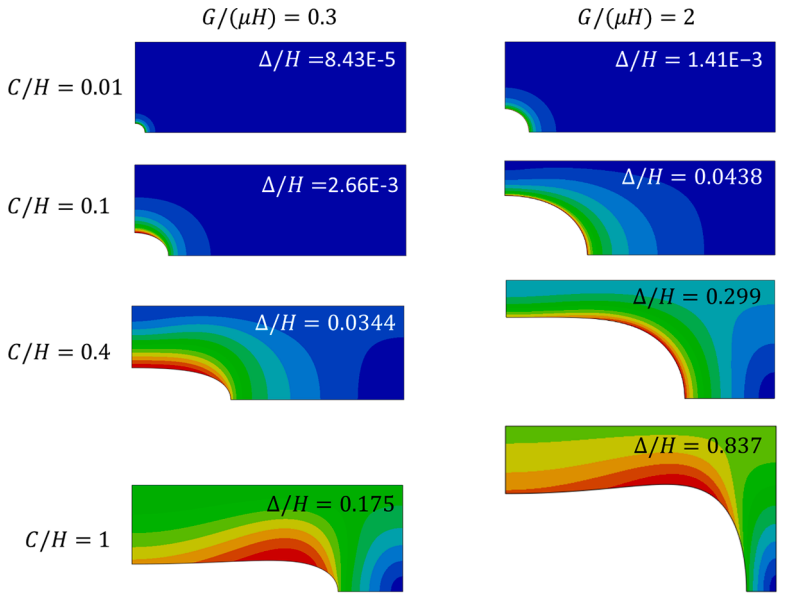

Fig. 7. Deformation of elastomer layers containing cracks of various radii. The energy release rate is $G/(\mu H) = 0.3$ in the left column, and is $G/(\mu H) = 2$ in the right column. Marked in each snapshot is the corresponding applied displacement. Color contours are for the amplitude of the displacement vector.

We compare elastomers of different values of toughness. In a brittle elastomer, $G_c/(\mu H) = 0.3$ (Fig. 7, the left column), the crack opening profile is close to a parabola, similar to that predicted by linear elasticity. By contrast, in a tough elastomer, $G_c/(\mu H) = 2$ (Fig. 7, the right column), the crack blunts significantly. For a crack arrested at a certain radius, the applied displacement is much larger for the tough elastomer than for the brittle elastomer. Correspondingly, the applied force is also higher (see the two dashed curves in Fig. 5a for the force-displacement curves).

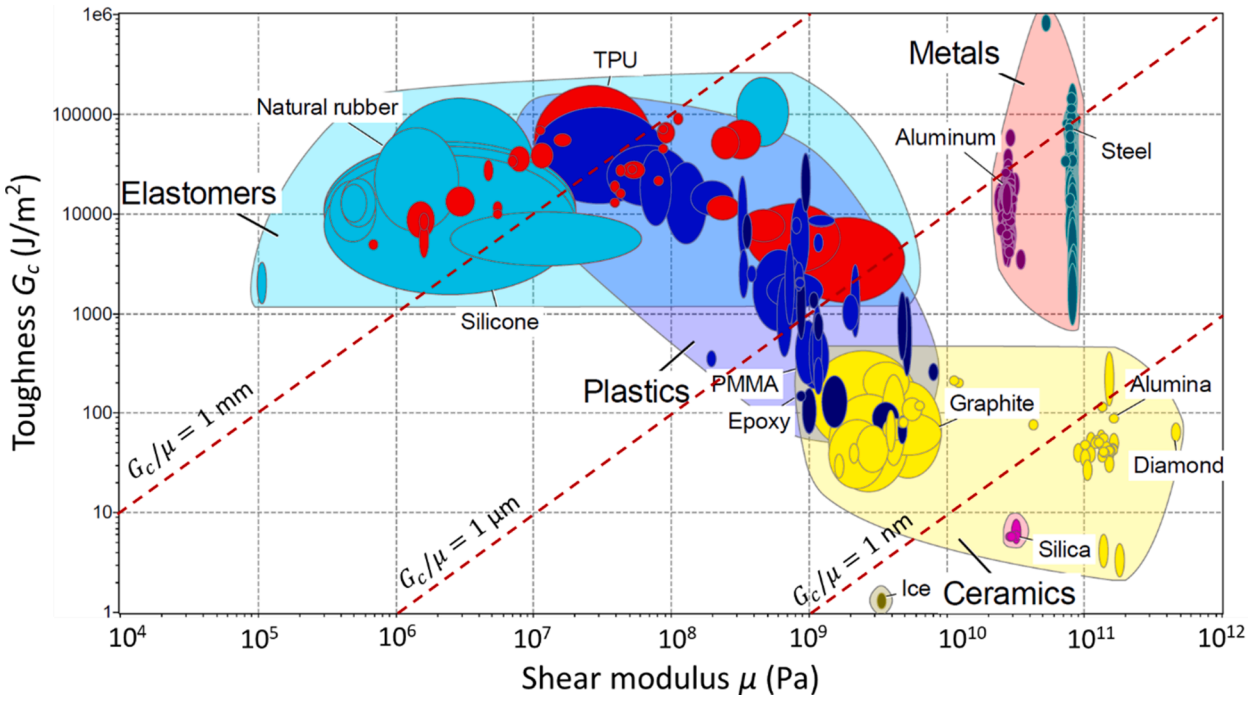

Fig. 8. A material bubble chart in the plane of shear modulus and toughness. Each type of material corresponds to a bubble on this plane. The dashed lines represent constant values of the material length G_c/μ, varying from ~0.1 nm (brittle, hard materials) to ~10 mm (tough, soft materials).

The normalized toughness, $G_c/(\mu H)$, is a ratio between two lengths: a material length G_c/μ and the elastomer thickness H. Similar material lengths have been identified before (e.g., Creton and Ciccotti, 2016). We show various materials on a plane of shear modulus and toughness (Fig. 8). On this plane, a constant value of the material length G_c/μ corresponds to a dashed line with a constant slope of 1. Depending on the materials, the length G_c/μ vary by many orders of magnitude, from 10^{-10} to 10^{-2} m. The material length is small for a brittle and stiff material, but large for a tough and soft material. For example, the material length G_c/μ is ~10 mm for natural rubber, and is ~0.1 mm for silicone. In comparison, the material length G_c/μ is less than 1 nm for silica glass, and is ~1 μm for a steel.

Due to the presence of the material length G_c/μ, which is fairly large for elastomers, the behavior of the elastomer layer is size dependent. Here we focus on situations in which the diameter of the specimen is much larger than the thickness, $D >> H$, so that the thickness of the elastomer, H, is the only relevant length other than the material length. If the thickness is small compared to the material length, $H < G_c/\mu$, the thin elastomer layer behaves like a tough material, for which the applied force can exceed the critical value for elastic instability, $F/(\pi B^2\mu) = 2.5$. However, if the thickness is larger than the material length, $H > G_c/\mu$, the elastomer layer behaves like a brittle material, with a peak force close to the critical value for elastic instability followed by a sharp drop of the force upon crack growth. The two types of force-displacement responses are illustrated by the two dashed lines in Fig. 5a for $G_c/(\mu H) = 2$ and 0.3, respectively.

In the experiments of Gent and Lindley (1959), a natural rubber was used. Assuming representative values for the rubber, $\mu \sim 0.5$ MPa and $G_c \sim 10^4$ J/m^2, the material length is $G_c/\mu \sim 2$ cm, which is much larger than the thickness of the thin specimens (< 1 mm) in their experiments. In a recent work by Guo and Ravi-Chandar (2022), a silicone was used in similar cavitation experiments. Assuming the shear modulus of the silicone is similar (~0.5 MPa), but the toughness is lower (~100 J/m^2), the material length in this case is $G_c/\mu \sim 0.2$ mm, which is smaller than the specimen thickness (~0.6 mm). The two sets of experiments reported apparently different force-displacement curves, resembling the tough and brittle responses, respectively.

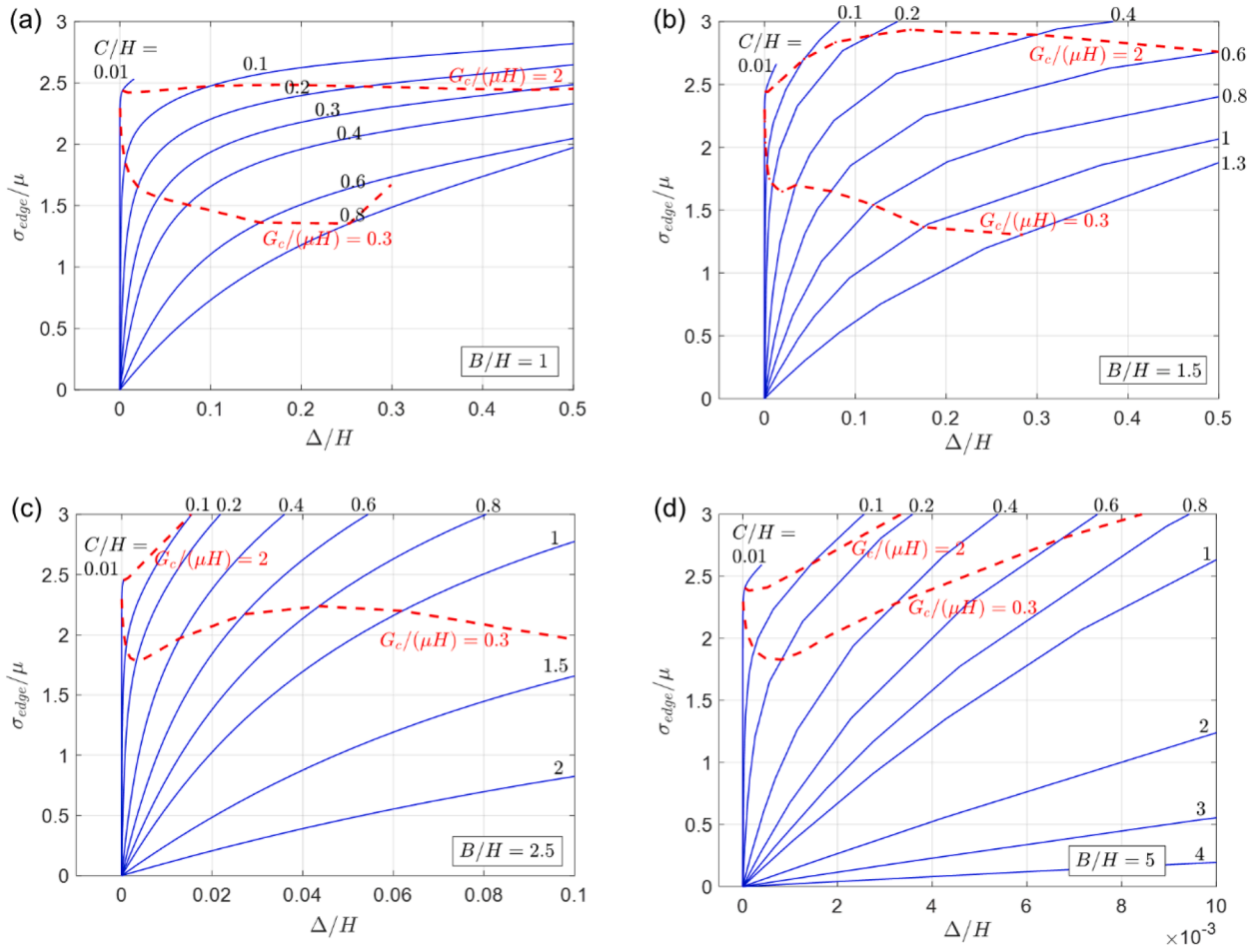

Fig. 9. Normalized hydrostatic stress at the edge of the axisymmetric model with different values of B/H. (a-d): $B/H = 1$, 1.5, 2.5, and 5. The solid lines are for fixed crack radii C/H, and the dashed lines are for constant energy release rates ($G = G_c$).

5. Crack spacing

The arrest of cracks makes it possible to have numerous small cracks in a thin elastomer layer ($D >> H$). Each crack relaxes the hydrostatic tension in a region around it, where other cracks cannot grow. When an existing crack arrests, far away from the crack, the hydrostatic tension is unrelaxed, so that new cracks can grow. In the axisymmetric model (Fig. 2), the spacing between adjacent cracks is represented approximately by the diameter $2B$. If B/H is large, the hydrostatic stress at the edge ($R = B$) may exceed the critical stress ($\sigma_c = 2.5\mu$), so that additional cracks may grow, reducing the crack spacing until the hydrostatic stress between the adjacent cracks is below the critical stress. Note that the value of B/H has negligible effect on the initiation of crack growth as long as the pre-existing crack is small ($C << H, B$).

The hydrostatic stress at the edge maximizes at the midplane, where we assume that new cracks will form if the critical hydrostatic stress is reached. The intersection between the edge and the midplane is in a state of triaxial stress of unequal components. Here, we assume that the critical condition for the formation of a new cavity is that the hydrostatic stress reaches 2.5μ. We will not consider the effect of triaxiality due to the unequal stress components (Long and Hui, 2010). We calculate the hydrostatic stress at the edge of the axisymmetric model as a function of the applied displacement Δ/H, for various values of C/H and four values of B/H (Fig. 9). For each pair of C/H and B/H, the hydrostatic stress σ_{edge} increases with the applied displacement and reaches the critical stress ($\sigma_c = 2.5\mu$) at a particular displacement Δ/H. At a constant displacement, the edge stress decreases with increasing crack radius. Also plotted on the same diagrams are contours of constant energy release rate (dashed curves), each corresponding to the case of a growing crack with a constant toughness ($G = G_c$). The dashed curve is generally not monotonic with the applied displacement, due to the simultaneously increasing crack radius that tends to decrease the edge stress. An intersection between a solid curve and a dashed curve represents an arrested crack. When the crack arrests, if the edge stress exceeds the critical stress, $\sigma_{edge} > \sigma_c$, we assume that a new crack will nucleate and grow in between of the existing cracks. For example, consider the two dashed contours for the model of $B/H = 1.5$ (Fig. 9b). The contour of $G_c/(\mu H) = 0.3$ intersects with the solid curves of various crack radii, all with the edge stress below the critical stress, $\sigma_{edge} < \sigma_c$, so that no new crack can form, and the spacing between the arrested cracks can be larger but not smaller than $2B/H = 3$. By contrast, the contour of $G_c/(\mu H) = 2$ intersects with the solid curves of various crack radii, with some intersections above the critical stress, $\sigma_{edge} > \sigma_c$, so that new cracks can form, and the spacing between the arrested cracks can be smaller but not larger than $2B/H = 3$.

Now consider all four panels in Fig. 9, corresponding to four values of B/H. For $G_c/(\mu H) = 0.3$, the edge stress drops below the critical stress ($\sigma_c = 2.5\mu$) upon crack growth for $B/H = 1$, 1.5 and 2.5, but rises up to above the critical stress for $B/H = 5$. In this case, the spacing between arrested cracks should be $5 < 2B/H < 10$. For $G_c/(\mu H) = 2$, the edge stress exceeds the critical stress for $B/H = 1.5$, 2.5 and 5, but remains below the critical stress for $B/H = 1$. In this case, the spacing between arrested cracks should be $2 < 2B/H < 3$. Therefore, the crack spacing ($\sim 2B/H$) decreases as the normalized toughness $G_c/(\mu H)$ increases, and a specimen with a large value of $G_c/(\mu H)$ ruptures by forming numerous small cracks with small spacing in between.

Moreover, the crack spacing depends on the applied displacement. As illustrated in Fig. 9(d) for $B/H = 5$ and $G_c/(\mu H) = 0.3$, the edge stress is below the critical stress when the applied displacement is small, but exceeds the critical stress when the applied displacement is large. Thus, the spacing between arrested cracks, $2B/H$, can be greater than 10 at a small displacement, but becomes less than 10 as the applied displacement increases, with additional crack formation between the existing cracks. For $B/H = 1$ and $G_c/(\mu H) = 0.3$ or 2 (Fig. 9a), the edge stress remains below the critical stress for much larger applied displacements, Δ/H up to 0.5. Further increasing the displacement would lead to even larger crack radius, with the crack front approaching the edge ($C \to B$), but the hydrostatic stress at the edge would remain below the critical stress. Consequently, the spacing between arrested cracks would not decrease further.

6. Concluding remarks

This paper studies why a thin layer of elastomer pulled by two rigid blocks grows numerous cracks using an idealized model. The model qualitatively answers the question, but quantitative comparison with experiments is challenging. The idealized model neglects several effects. First, the strain stiffening of the elastomer could suppress the elastic instability and thus delay the initiation of crack growth. Second, the surface energy γ introduces a material-specific length, γ/μ, which influences the nucleation and growth of small cavities (Gent and Tompkins, 1969; Kundu and Crosby, 2009). Third, the resistance to crack growth is typically not a constant, but increases with the crack growth (Thomas, 1958). The crack resistance curve (i.e., the energy release rate as a function of crack growth) defines yet another material-specific length. Fourth, the ratio between the toughness and the work of fracture, G_c/W_f, also defines a material-specific length (Yang et al., 2019; Kim et al., 2020). Thus, the idealized model in this study is valid in the limit when the elastomer deviates from the neoHookean material only at a large stretch, and when the initial crack radius is larger than the three material-specific lengths identified above. Moreover, the idealized model does not take into account the effect of loading rate, which could be important in experiments because many elastomers are viscoelastic.

In summary, we analyze an axisymmetric model of a finite radius, in which the elastomer contains a penny-shaped crack. The elastomer is taken to be an incompressible, neoHookean material. For a given applied displacement, we calculate the applied force, the energy release rate, and the hydrostatic stress at the edge of the elastomer. These results allow us to discuss initiation, growth, and arrest of the crack. The arrest of the crack makes it possible to have numerous cracks in a thin elastomer layer. The model also estimates the spacing between the cracks, which depends on the fracture toughness of the elastomer and the applied displacement. New cracks initiate if the hydrostatic stress at the edge of the elastomer exceeds a critical stress dictated by elastic instability. For an elastomer of thickness H, shear modulus μ, and toughness G_c, the elastomer layer grows numerous small cracks when the dimensionless parameter $G_c/(\mu H)$ is large. This prediction is qualitatively consistent with experiments.

CRediT authorship contribution statement

Sida Hao: Methodology, Investigation, Validation, Visualization, Writing – original draft. **Zhigang Suo:** Conceptualization, Methodology, Writing – review & editing. **Rui Huang:** Conceptualization, Methodology, Supervision, Visualization, Writing – review & editing.

Declaration of Competing Interest

The authors declare that they have no known competing financial interests or personal relationships that could have appeared to influence the work reported in this paper.

Data availability

Data will be made available on request.

Acknowledgments

S.H. and R.H. gratefully acknowledge financial support by the Portuguese Foundation for Science and Technology – FCT under the UT Austin Portugal program through the project Soft4Sense. Z. S. acknowledges the support of Harvard MRSEC (DMR-2011754) and of the Air Force Office of Scientific Research (FA9550-20-1-0397).

References

Barney, C.W., Dougan, C.E., McLeod, K.R., Kazemi-Moridani, A., Zheng, Y., Ye, Z., Tiwari, S., Sacligil, I., Riggleman, R.A., Cai, S., Lee, J.-.H., Peyton, S.R., Tew, G.N., Crosby, A.J., 2020. Cavitation in soft matter. PNAS 117, 9157–9165.
Creton, C., Ciccotti, M., 2016. Fracture and adhesion of soft materials: a review. Rep. Prog. Phys. 79, 046601.
Gent, A.N., 1990. Cavitation in rubber: a cautionary tale. Rubber Chem. Technol. 63, G49–G53.
Gent, A.N., Lindley, P.B., 1959. Internal rupture of bonded rubber cylinders in tension. Proc. R. Soc. Lond. A249, 195–205.
Gent, A.N., Tompkins, D.A., 1969. Surface energy effects for small holes or particles in elastomers. J. Polym. Sci. Part A-2 7, 1483–1488 vol.
Gent, A.N., Wang, C., 1991. Fracture mechanics and cavitation in rubber-like solids. J. Mater. Sci. 26, 3392–3395.
Guo, J. and Ravi-Chandar, K., 2022. On crack nucleation and propagation in elastomers: I. *In situ* optical and x-ray experimental observations. In review.
Hutchens, S.B., Fakhouri, S., Crosby, A.J., 2016. Elastic cavitation and fracture via injection. Soft Matter 12, 2557–2566.
Kang, J., Wang, C., Cai, S., 2017. Cavitation to fracture transition in a soft solid. Soft Matter 13, 6372–6376.
Kim, J.Y., Liu, Z., Weon, B.M., Cohen, T., Hui, C.-.Y., Dufresne, E.R., Style, R.W., 2020. Extreme cavity expansion in soft solids: damage without fracture. Sci. Adv. 6, eaaz0418.
Kumar, A., Lopez-Pamies, O., 2021. The poker-chip experiments of Gent and Lindley (1959) explained. J. Mech. Phys. Solids 150, 104359.
Kundu, S., Crosby, A.J., 2009. Cavitation and fracture behavior of polyacrylamide hydrogels. Soft Matter 5, 3963–3968.
Lefèvre, V., Ravi-Chandar, K., Lopez-Pamies, O., 2015. Cavitation in rubber: an elastic instability or a fracture phenomenon? Int. J. Fract. 192, 1–23.
Lin, Y.Y., Hui, C.Y., 2004. Cavity growth from crack-like defects in soft materials. Int. J. Fract. 126, 205–221.
Long, R., Hui, C.Y., 2010. Effects of triaxiality on the growth of crack-like cavities in soft incompressible elastic solids. Soft Matter 6, 1238–1245.
Morelle, X.P., Sanoja, G.E., Castagnet, S., Creton, C., 2021. 3D fluorescent mapping of invisible molecular damage after cavitation in hydrogen exposed elastomers. Soft Matter 17, 4266–4274.
Poulain, X., Lefèvre, V., Lopez-Pamies, O., Ravi-Chandar, K., 2017. Damage in elastomers: nucleation and growth of cavities, micro-cracks, and macro-cracks. Int. J. Fract. 205, 1–21.
Raayai-Ardakani, S., Chen, Z., Earl, D.R., Cohen, T., 2019a. Volume-controlled cavity expansion for probing of local elastic properties in soft materials. Soft Matter 15, 381–392.
Raayai-Ardakani, S., Earl, D.R., Cohen, T., 2019b. The intimate relationship between cavitation and fracture. Soft Matter 15, 4999–5005.
Thomas, A.G., 1958. Rupture of Rubber. V. cut growth in natural rubber vulcanizates. J. Polymer Sci. XXXI, 467–480.
Williams, M.L., Schapery, R.A., 1965. Spherical flaw insensitivity in hydrostatic tension. Int. J. Fract. Mech. 1, 64–71.
Yang, C., Yin, T., Suo, Z., 2019. Polyacrylamide hydrogels. I. Network imperfection. J. Mech. Phys. Solids 131, 43–55.